Catalysis Science & Technology

PAPER

View Article Online
View Journal

Cite this: DOI: 10.1039/c6cy00118a

FePd alloy nanoparticles assembled on reduced graphene oxide as a catalyst for selective transfer hydrogenation of nitroarenes to anilines using ammonia borane as a hydrogen source†

Önder Metin,*[a] Adriana Mendoza-Garcia,[b] Diğdem Dalmızrak,[a] Mehmet Serdar Gültekin[a] and Shouheng Sun*[b]

Received 17th January 2016,
Accepted 8th May 2016

DOI: 10.1039/c6cy00118a

www.rsc.org/catalysis

Addressed herein is a facile protocol for the synthesis and assembly of FePd alloy nanoparticles (NPs) on reduced graphene oxide (rGO) to catalyze transfer hydrogenation of nitroarenes to anilines under ambient conditions. 3.5 nm FePd NPs were synthesized by using a surfactant-assisted co-reduction method that allowed NP composition control. FePd NPs were then assembled on rGO *via* a liquid-phase self-assembly method and studied as catalysts to promote hydrogen transfer from ammonia borane (AB) to numerous nitroarenes in aqueous methanol solutions at room temperature. Among three different rGO–FePd, the commercial C–Pd and rGO–Pd catalysts tested, rGO–$Fe_{48}Pd_{52}$ showed the highest efficiency in converting nitroarenes to anilines, achieving >90% yields within 10–20 min of reactions. Our work demonstrates an efficient and selective approach to transfer hydrogenation of nitroarenes to anilines.

Introduction

Transition metal nanoparticles (NPs) have been widely used as catalysts in various reactions owing to their distinct properties compared to bulk metals, filling the gap between homogeneous and heterogeneous catalysts.[1] Recent trends in nanocatalysis have proposed the use of bimetallic NPs, which comprise two distinct transition metal atoms in various configurations[2] because they show considerably different properties when compared to their monometallic analogues.[3] One typical example is in catalysis where bimetallic alloy NPs show synergistic effects that arise from the interaction of two distinct metals.[4,5] These bimetallic alloy NPs not only provide higher catalytic activity and selectivity than their monometallic counterparts but also allow one to minimize the use of expensive noble metals in the catalyst components.[6] Recently, a variety of noble metal alloy NPs have been studied as catalysts for various chemical reactions,[7] and those based on palladium (Pd) are especially popular due to the known Pd catalysis in various organic reactions.[8]

We have recently reported the synthesis of monodisperse CoPd,[9] NiPd[10] and CuPd[9,11] alloy NPs and studied their catalysis in different reactions. One reaction was the transfer hydrogenation to convert nitroarenes/nitriles to anilines (Ar–NH_2), which are important precursors for the synthesis of colorants and antioxidants, as well as the key intermediates in the fine chemical, agrochemical, and pharmaceutical industries.[12] Conventionally, Ar–NH_2 compounds are prepared by direct hydrogenation of nitroarenes (Ar–NO_2) or aromatic nitriles (Ar–CN).[13,14] However, these hydrogenation reactions require the use of high-pressure hydrogen gas and high temperatures.[15] Recent studies on hydrogenation reactions have been directed to the development of transfer hydrogenation in which hydrogen is generated *in situ* from a donor molecule and transferred to the substrate with the help of a catalyst.[16] The donor molecule can be hydrazine,[17] isopropanol,[18] glycerol[19] or formic acid,[20] but the hydrogenation kinetics from these donor molecules are slow, providing low product yields under ambient conditions. Our recent studies show that ammonia borane complex (AB, H_3NBH_3) can be used as a hydrogen reservoir[21] for transfer hydrogenation of Ar–NO_2 and Ar–CN to the corresponding amines in the presence of graphene supported MPd (M = Co or Ni) NPs.[9,22] The hydrogenation reaction provides not only high amine yields (>90%) in <20 min but also the desired selectivity towards nitro moieties in aromatic compounds.

To complete our studies on the MPd alloy series, here we report the synthesis of FePd NPs and their catalysis in the

[a] Department of Chemistry, Faculty of Science, Atatürk University, Erzurum 25240, Turkey. E-mail: ometin@atauni.edu.tr
[b] Department of Chemistry, Brown University, Providence, Rhode Island 02912, USA. E-mail: ssunn@brown.edu

† Electronic supplementary information (ESI) available. See DOI: 10.1039/c6cy00118a

transfer hydrogenation of Ar–NO_2 using AB as a hydrogen source in a water–methanol solvent mixture at room temperature. Following a procedure that is similar to our previous synthesis of MPd alloy NPs, we prepared 3.5 nm FePd NPs by co-reduction of iron(III) acetylacetonate and palladium(II) acetylacetonate with a morpholine borane complex (MB) in a mixture of oleylamine (OAm) and 1-octadecene (ODE) at 100 °C. Three different kinds of FePd NPs, namely, $Fe_{39}Pd_{61}$, $Fe_{48}Pd_{52}$ and $Fe_{62}Pd_{38}$ NPs, supported on reduced graphene oxide (rGO), as well as metallic Pd NPs, were studied. Our tests showed that rGO–$Fe_{48}Pd_{52}$ was the most efficient catalyst in converting nitroarenes to anilines under the optimized conditions.

Results and discussion

We have recently reported the synthesis of monodisperse MPd (M: Co,[9] Ni,[10] and Cu[11]) alloy NPs and their successful catalysis in various reactions after supporting them on rGO. In these established protocols, MPd alloy NPs were synthesized by the co-reduction of metal precursors with borane-based mild reducing agents (morpholine borane (MB) for CuPd or borane-*tert*-butylamine for NiPd and CoPd NPs in the presence of oleylamine (OAm) and 1-octadecene (ODE)). FePd NPs were previously synthesized in the presence of phosphine- and sulfur-based surfactants,[23] but these surfactants were difficult to remove from the NP surface after the synthesis. We modified the protocols for the synthesis of CuPd NPs and prepared FePd NPs by using OAm as the sole surfactant. The composition of the NPs was controlled by the metal salt ratio during the synthesis and was determined by ICP-AES analysis. Fig. 1A shows a representative TEM image of the as-prepared $Fe_{48}Pd_{52}$ NPs. Although the shapes of $Fe_{48}Pd_{52}$ NPs are not completely uniform, they have a narrow size distribution with an average of 3.5 ± 0.5 nm. The HRTEM image of a single FePd NP (Fig. 1B) shows the polycrystalline nature of the NP with a (111) lattice fringe distance of 0.211 nm, which is smaller than that of the Pd metal (0.223 nm), indicating the Fe alloying effect on the lattice reduction in the alloy structure. The XRD pattern of the FePd NPs (Fig. 1C) also supports the formation of the alloy, as the (111) peak right-shifts 1.2° ($FePd_{2\theta}$ = 40.8° *vs.* $Pd_{2\theta}$ = 39.6°). The size of the FePd NPs was estimated by the Scherrer equation[24] as 3.1 nm, which is smaller than the one obtained from the TEM image analysis and indicative of the polycrystalline nature of the NPs.

In addition to the $Fe_{48}Pd_{52}$ NPs, $Fe_{39}Pd_{61}$ and $Fe_{62}Pd_{38}$ NPs were also synthesized so that Fe/Pd composition dependent catalysis could be studied. The $Fe_{39}Pd_{61}$ NPs were obtained by mixing 0.2 mmol of $Fe(acac)_3$ and 0.3 mmol of $Pd(acac)_2$ and $Fe_{62}Pd_{38}$ NPs were synthesized using 0.3 mmol of $Fe(acac)_3$ and 0.2 mmol of $Pd(acac)_2$. Fig. 2 shows representative TEM images of the $Fe_{39}Pd_{61}$ and $Fe_{62}Pd_{38}$ NPs.

They are similar in size (4 ± 0.5 and 3.8 ± 0.4 nm, respectively) and shape to the $Fe_{48}Pd_{52}$ NPs. Monodisperse Pd NPs were also prepared by the OAm mediated synthesis protocol reported elsewhere[25] and used as the control.

To study the NP catalysis for transfer hydrogenation reactions, we assembled the FePd NPs and Pd NPs on the rGO (abbreviated as rGO–FePd and rGO–Pd hereafter). Here, the rGO was chosen as the support material because it has been demonstrated that its 2D structure can promote the adsorption of the organic substrates around the catalyst, making the interaction between the substrates and the NPs more effective.[10,11,22] Representative TEM images of the rGO–$Fe_{48}Pd_{52}$ catalysts taken at different magnifications (Fig. 3) and rGO–Pd (Fig. S1†) indicate that the deposition of the NPs on the rGO does not change the NP morphology, and the NPs are well dispersed on the rGO surface without any sign of agglomeration. The rGO–$Fe_{48}Pd_{52}$, or the other rGO–FePd, has 16% wt of FePd as measured by ICP-AES analyses.

The rGO–$Fe_{48}Pd_{52}$ catalyst was further analyzed by X-ray photoelectron spectroscopy (XPS). The survey XP spectrum of the rGO–$Fe_{48}Pd_{52}$ (Fig. S2†) shows the existence of elements C, O, N, Fe and Pd that are from the rGO, OAm and FePd NPs. The Fe 3p (700–730 eV) and Pd 3d (330–345 eV) regions were also examined (Fig. 4). Two main peaks are observable in the Fe 3p region (Fig. 4A) at 708.7 and 720.5 eV, indicating that Fe atoms are in the metallic state.[26,27] The Pd 3d spectrum

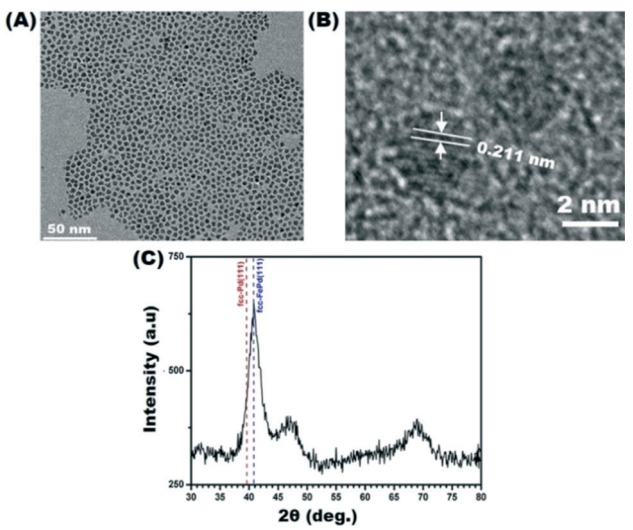

Fig. 1 (A) TEM image, (B) HRTEM image and (C) XRD pattern of the $Fe_{48}Pd_{52}$ NPs.

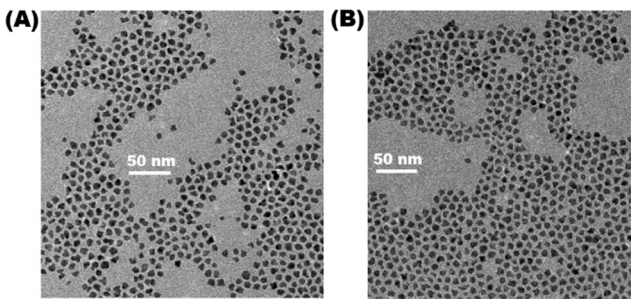

Fig. 2 Representative TEM images of (A) $Fe_{39}Pd_{61}$ and (B) $Fe_{62}Pd_{38}$ NPs.

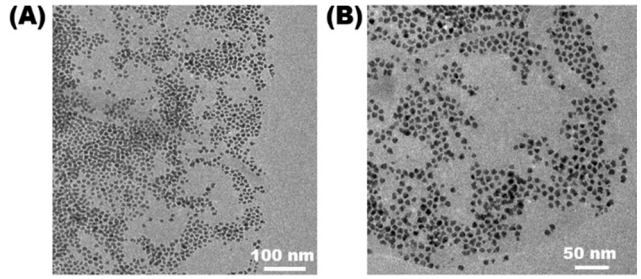

Fig. 3 Representative TEM images of the $Fe_{48}Pd_{52}$ NPs supported on rGO (rGO–$Fe_{48}Pd_{52}$).

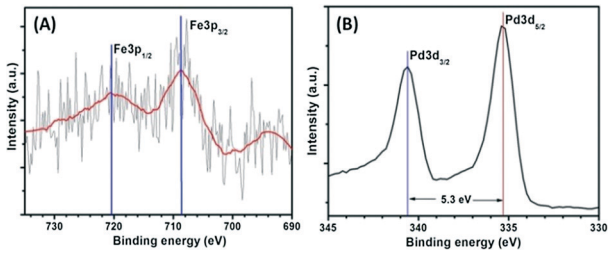

Fig. 4 XPS of the rGO–$Fe_{48}Pd_{52}$ in the (A) Fe 3p and (B) Pd 3d regions.

shows two peaks at 335.3 and 340.6 eV that can be assigned to metallic Pd.[28] From this study, we cannot observe the oxidized Fe species in the Fe 3p spectrum, which further infers that alloying Fe with Pd prevents Fe from deep oxidation.

We studied the transfer hydrogenation reactions to nitroarenes in the presence of rGO–FePd or rGO–Pd and AB. After screening a range of conditions using rGO–$Fe_{48}Pd_{52}$ as the catalyst and nitrobenzene as the substrate, we found that aniline was obtained with a >99% yield (Table 1, entry 1) in the conditions similar to what we have reported on the rGO–$Ni_{30}Pd_{70}$[10] and rGO–$Co_{30}Pd_{70}$[22] catalytic reactions. Therefore, we used these conditions, namely, 1 mmol of substrate, 3 mmol of AB and 5 mg of catalyst in a water–methanol solvent mixture (10 mL, v/v = 3/7) at room temperature to study the transfer hydrogenation reactions.

As the control, we performed the transfer hydrogenation reactions on nitrobenzene without any catalyst component or in the presence of pristine rGO, or rGO–Pd, or the commercial C–Pd catalyst. The test results are listed in Table 1, entries 2–7. Without any catalyst component or with only pristine rGO present, the reaction did not lead to any observable conversion. Even after 12 h of reaction, the conversion yield was still <5%. When C–Pd or rGO–Pd was present, the conversion yield reached 75% or 78%, respectively. However, the selectivity of either C–Pd or rGO–Pd towards aniline was poor (10% for the C–Pd and 15% for the rGO–Pd) due to the formation of other by-products.[29] We further studied the alloy effect on the catalytic activity (Table 1). The tests indicate that alloying Pd with Fe improves Pd catalytic activity and selectivity for the transfer hydrogenation reaction, and the rGO–$Fe_{48}Pd_{52}$ catalyst shows the best activity and selectivity.

Pd is well known as a good hydrogenation catalyst.[30] Fe(0) has also been studied as a catalyst for the hydrogenation of nitrobenzene to aniline in aqueous media under anaerobic conditions.[31] In the reaction, Fe corrosion cannot be prevented, and as a result, the hydrogenation rate is quickly decreased. By alloying Fe with Pd to induce charge transfer from Fe to Pd, Fe is much better stabilized and Pd sites become more electron-rich, facilitating Ar–NO_2 adsorption and hydrogenation reactions (the ensemble and ligand effect).[32] From this pure charge transfer argument, we may conclude that more Fe present in the FePd alloy structure should be better for catalysis. However, too much Fe can lead to the noticeable lattice reduction within the solid solution structure, lowering hydrogen solubility in Pd[33] and slowing down the hydrogenation kinetics. Therefore, for the reported transfer hydrogenation reaction, FePd alloy NPs need to have an optimum composition to show substantially enhanced catalysis. For the FePd NPs studied in this paper, the optimum composition is $Fe_{48}Pd_{52}$.

The preparative scope of rGO–$Fe_{48}Pd_{52}$ catalyzed transfer hydrogenation reactions was further investigated and summarized in Table 2. Some representative nitroarenes (entries 1–15) were converted to the corresponding anilines in excellent yields within time periods between 10–20 min at room temperature. As the first example, the benchmark substrate nitrobenzene (1) was hydrogenated to give aniline (2) with a stoichiometric yield in 10 min (Table 2, entry 1). To

Table 1 Screening of transfer hydrogenation reactions

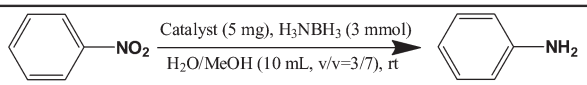

Entry	Catalyst	Yield[a] (%)	Selectivity[b] (%)	Time
1	rGO–$Fe_{48}Pd_{52}$	>99	>99	15 min
2	—	<5	—	12 h
3	C–Pd	75	10[c]	15 min
4	rGO–Pd	78	15[c]	15 min
5	rGO–$Fe_{39}Pd_{61}$	90	40[c]	15 min
6	rGO–$Fe_{62}Pd_{38}$	95	8[c]	15 min
7	rGO	<5	—	12 h

[a] Conversion yields under the reaction conditions: 1 mmol of substrate, 3 mmol of NH_3BH_3, 5 mg of catalyst, 10 mL of water–methanol solvent mixture (v/v = 3/7), rt. [b] Selectivity towards aniline. [c] See the ESI for product analysis by ^1H and ^{13}C-NMR spectra.

Table 2 The scope of rGO–$Fe_{48}Pd_{52}$ catalyzed transfer hydrogenation reactions using ammonia borane as a hydrogen source

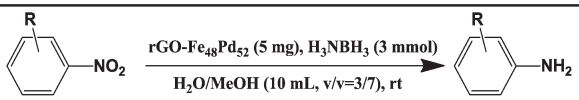

Entry	Substrate	Product	Yield[a] (%)	Time (min)
1	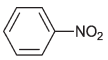 (1)	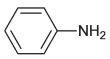 (2)	>99	10
2	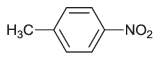 (3)	 (4)	>99	10
3	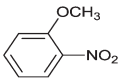 (5)	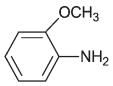 (6)	>99	10
4	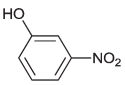 (7)	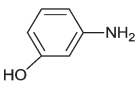 (8)	>99	10
5	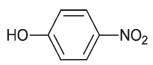 (9)	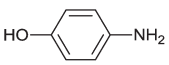 (10)	>99	10
6	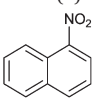 (11)	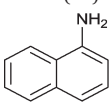 (12)	>99	15
7	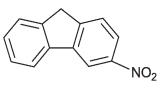 (13)	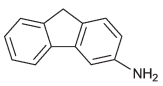 (14)	>99	15
8	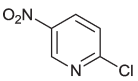 (15)	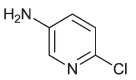 (16)	>99	15
9	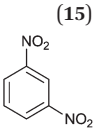 (17)	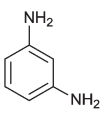 (18)	>99	15
10	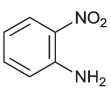 (19)	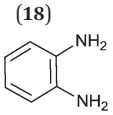 (20)	>99	15
11	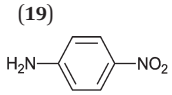 (21)	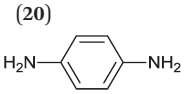 (22)	>99	15
12	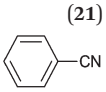 (23)	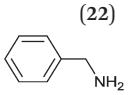 (24)	95	15
13	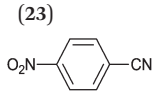 (25)	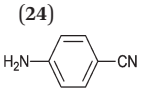 (26)	>99	10
14	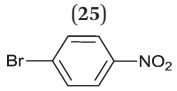 (27)	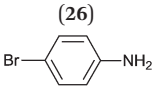 (28)	>99	15
15	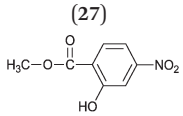 (29)	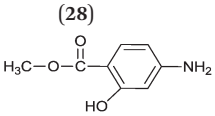 (30)	90	15

[a] Reaction conditions: 1 mmol of substrate, 3 mmol of NH_3BH_3, 5 mg of rGO–$Fe_{48}Pd_{52}$ catalyst, 10 mL of water–methanol solvent mixture (v/v = 3/7), rt.

understand the substituent tolerance of the catalytic transfer hydrogenation reaction, we tested it on the conversion of nitrobenzenes bearing various electron donor or withdrawing substituents (**3**, **5**, **7**, and **9**), which were all converted to relevant anilines (**4**, **6**, **8**, and **10**) quantitatively (Table 2, entries 2–5). The rGO–$Fe_{48}Pd_{52}$ catalyst was successfully applied for the near quantitative reduction of more complex aromatic nitro compounds (**11**, **13** and **15**) to the corresponding aniline derivatives (**12**, **14**, **16**) in 15 min (Table 2, entries 6–8). The transfer hydrogenation reaction could also be used to reduce aromatic compounds bearing two $-NO_2$ groups at *meta*- (**17**), *ortho*- (**19**) and *para*- (**21**) positions to the corresponding diamines (**18**, **20**, and **22**) in 15 min (Table 2, entries 9–11).

The transfer hydrogenation reaction catalyzed by rGO–$Fe_{48}Pd_{52}$ could be extended to the reduction of Ar–CN. Under the same reaction conditions, benzonitrile (**23**) was converted to benzylamine (**24**) in 15 min with a yield of 95% (Table 2, entry 12). However, when 4-nitro-benzonitrile (**25**) was a substrate, only the $-NO_2$ was reduced to $-NH_2$ (**26**), while –CN stayed intact (Table 2, entry 13). This is very similar to the transfer hydrogenation on the rGO–$Ni_{30}Pd_{70}$[10] and rGO–$Co_{30}Pd_{70}$[22] catalysts, indicating a general case of rGO–MPd (M: Fe, Co, Ni) on the selective reduction of $-NO_2$ over –CN in the *p*-NH_2-C_6H_4-CN structure. When other groups susceptible to reduction are present, such as in 1-bromo-4-nitrobenzene (**27**) and methyl 2-hydroxy-4-nitrobenzoate (**29**), the hydrogenation reaction led to the formation of the related amine products (>99%, 5 min) (Table 2, entries **14** and **15**) and the Br- or ester groups were not affected.

We tested the efficiency of the rGO–$Fe_{48}Pd_{52}$ catalyst for transfer hydrogenation by running a scale-up reaction containing 10 mmol of nitrobenzene with other reaction components increased at the same ratios. After the first round of reaction, we obtained aniline in 98% yield. After five consecutive runs of the same reaction, the catalyst showed only a slight decrease in activity with the aniline yield staying at 95%. Once separated from the reaction mixture and washed with the clean methanol/water solvent, the catalyst was analyzed again by TEM and XRD. Fig. S3† shows the TEM image and XRD pattern of the rGO–$Fe_{48}Pd_{52}$ catalyst after the 5th round of reaction. From the TEM image (Fig. S3A†), we see neither agglomeration nor obvious deformation of the NPs. The XRD pattern of the catalyst shows that the alloy peak still dominates the catalyst phase and there are no oxides detected (Fig. S3B†). The studies indicate that the rGO–$Fe_{48}Pd_{52}$ catalyst is not only active for the transfer hydrogenation reaction but also durable under the reaction conditions.

Conclusions

We report a facile route for the synthesis of 3.5 nm FePd NPs and their assembly on rGO. The rGO–$Fe_{48}Pd_{52}$ catalyst is highly efficient at room temperature in catalyzing hydrogenation of nitroarenes to anilines (>90% yield in ≤20 min) with AB as the hydrogen source. Compared to our previous reports on the same transfer hydrogenation reactions in the presence of rGO–NiPd and rGO–CoPd catalysts, the rGO–FePd performance lies between rGO–NiPd and rGO–CoPd with the rGO–CoPd being the most efficient in terms of reaction times required to complete the reaction. Moreover, the rGO–$Fe_{48}Pd_{52}$ catalyst is also highly durable under the reaction conditions. We can conclude that alloying Pd with Fe (or Co, or Ni) can indeed enhance Pd catalysis for transfer hydrogenation reactions using AB as a hydrogen donor in the water–methanol mixture. The rGO–FePd catalyst and other rGO–MPd catalysts represent a new class of catalyst that can be used to achieve efficient and selective hydrogenation reactions for the reduction of R–NO_2 and R–CN to Ar–NH_2 in a green chemistry environment.

Experimental section

Materials

Iron(III) acetylacetonate ($Fe(acac)_3$, 99%), palladium(II) acetylacetonate ($Pd(acac)_2$, 99%), oleylamine (OAm, >70%), 1-octadecene (ODE), ethyl alcohol (99%), hexane (97%), potassium permanganate ($KMnO_4$, >99%), sodium nitrate ($NaNO_3$, >99%), dimethylformamide (DMF, >99%) and all nitroarenes tested in the transfer hydrogenation reactions were purchased from Sigma-Aldrich®. Hydrogen peroxide (H_2O_2, 30%) and sulfuric acid (H_2SO_4, 95–98%) were purchased from Merck®. Natural graphite flakes (average particle size 325 mesh) and morpholine borane complex (MB, 97%) were purchased from Alfa Aesar®. Milli-Q deionized water was used in all catalytic experiments.

Instrumentation

TEM images were obtained using a FEI Technai G^2 Spirit BiO(TWIN) instrument operating at 120 kV. HRTEM images were acquired using a JEOL 2100F operating at 200 kV. XRD patterns were collected using a Bruker AXS D8-Advanced diffractometer with Cu Kα radiation (λ = 1.5418 Å). X-Ray photoelectron spectroscopy (XPS) measurements were performed using a SPECS XP spectrometer (Germany) equipped with a PHOIBOS hemispherical energy analyser. A monochromatic Al Kα X-ray excitation ($h\nu$ = 1486.74 eV, 350 W) source was employed in the XPS data acquisition. Binding energy (BE) calibration of the XP spectra were carried out with the help of the amorphous carbon C 1s signal located at 284.6 eV. ICP-AES measurements were carried out using a JY2000 Ultrace ICP Atomic Emission Spectrometer equipped with a JY AS 421 autosampler and a 2400 g mm^{-1} holographic grating. Each sample was completely dissolved in aqua regia (HCl/HNO_3, 3/1 v/v ratio) prior to analysis. ^{1}H-NMR and ^{13}C-NMR spectra were obtained by using a Bruker Avance DPX 400 MHz spectrometer.

Synthesis of FePd and Pd NPs

The synthesis of NPs was performed by using standard inert atmosphere procedures and commercially available reagents.

In a typical synthesis of $Fe_{48}Pd_{52}$ NPs, 0.25 mmol of $Pd(acac)_2$ and 0.25 mmol of $Fe(acac)_3$ were dissolved in 3 mL of OAm in a glass vial. Separately, 0.2 g of MB was dissolved in OAm (3 mL) and ODE (7 mL) in a four-necked round bottom flask. Next, the metal precursor mixture was quickly injected into the reactor at 100 °C under vigorous stirring. After injection, the color of the solution turned dark brown indicating the co-reduction of Pd(II) and Fe(III) ions and the formation of alloy NPs. The reaction solution was kept at this temperature for 1 h before it was cooled down to room temperature. An acetone/ethanol mixture (v/v = 7/3) was added to precipitate out the product, and the NPs were separated by centrifugation at 9000 rpm for 12 min. The NP product was redispersed in hexane and precipitated by ethanol. After centrifugation, the solvent was discarded and the NPs were dispersed in hexane and kept for further use.

By changing the ratio of the metal precursors, two other compositions of FePd NPs were synthesized using the same protocol. To obtain $Fe_{39}Pd_{61}$ NPs, 0.2 mmol of $Fe(acac)_3$ and 0.3 mmol of $Pd(acac)_2$ were used, while to synthesize $Fe_{62}Pd_{38}$ NPs, 0.3 mmol of $Fe(acac)_3$ and 0.2 mmol of $Pd(acac)_2$ were used.

The monodisperse Pd NPs were synthesized by using the reported method.[25]

Synthesis of reduced graphene oxide (rGO)

rGO was prepared by using well-established procedures. First, graphene oxide (GO) was prepared *via* modified Hummer's method.[34] Next, GOs were reduced by refluxing them in a DMF solution for 6 h.[35] Details of the synthesis procedure and characterization of rGO can be found in our previous report.[36]

Supporting NPs on rGO

In a typical procedure, 40 mg of rGO was dispersed in 40 mL of ethanol (1 mg ml^{-1}) *via* sonication, and then 20 mg of the hexane dispersion of FePd NPs was added. The final mixture was sonicated for 2 h to assemble the FePd NPs on the rGO. The rGO–FePd was separated by centrifugation at 7500 rpm for 12 min and then purified by washing twice with ethanol and dried under vacuum. The same procedure was applied to support Pd NPs on rGO.

General procedure for the transfer hydrogenation reactions

All catalytic transfer hydrogenation reactions were performed in a 38 mL thermolysis tube under air atmosphere as described in our previous reports.[10,22] In a typical catalytic transfer hydrogenation reaction, 1 mmol of substrate and 5 mg of rGO–FePd catalyst were mixed in 10 mL of water–methanol solvent mixture (v/v = 3/7) inside the thermolysis tube for 10 min at room temperature. Next, 3 mmol of H_3NBH_3 (AB) were added to the reaction mixture and the reaction was started by closing the thermolysis tube tightly. Next, the reaction was continued under vigorous stirring at room temperature and the progress of the catalytic reaction was monitored by thin layered chromatography (TLC). Most of the reactions were completed within 10–20 min. Upon reaction completion, the catalysts were separated by centrifugation and cleaned several times using a water/methanol mixture. The reaction products were purified by first evaporating the solvents using a rotary evaporator and secondly passing through the silica gel column using acetone/*n*-hexane (1 : 4) as an eluent. The yields of anilines were determined by ^{1}H-NMR and ^{13}C-NMR, and the purified products were dissolved in D_2O, d^6-DMSO, CD_3OD or $CDCl_3$ depending on the product solubility. Please see the supporting information of our previous paper for the ^{1}H-NMR and ^{13}C-NMR spectra of the purified amine products.[10]

Acknowledgements

This work was mostly conducted at the Department of Chemistry, Atatürk University and financially supported by the Scientific and Technological Research Council of Turkey (TUBITAK, Project No. 113Z276). The part conducted at Brown University was supported by the U.S. Army Research Laboratory and the U.S. Army Research Office under the Multi University Research Initiative (MURI, grant number W911NF-11-1-0353) on "Stress-Controlled Catalysis *via* Engineered Nanostructures".

Notes and references

1 (*a*) D. Astruc, *Inorg. Chem.*, 2007, **46**, 1884; (*b*) J. D. Aiken III and R. G. Finke, *J. Mol. Catal. A: Chem.*, 1999, **145**, 1.
2 D. Wang and Y. Li, *Adv. Mater.*, 2011, **23**, 1044.
3 (*a*) N. Toshima and T. Yonezawa, *New J. Chem.*, 1998, **22**, 1179; (*b*) S. E. Habas, H. Lee, V. Radmilovic, G. A. Somorjai and P. Yang, *Nat. Mater.*, 2007, **6**, 692; (*c*) D. Xu, Z. P. Liu, H. Z. Yang, Q. S. Liu, J. Zhang, J. Y. Fang, S. Z. Zou and K. Sun, *Angew. Chem., Int. Ed.*, 2009, **48**, 4217–4221.
4 M. Sankar, N. Dimitratos, P. J. Miedziak, P. P. Wells, C. J. Kielye and G. J. Hutchings, *Chem. Soc. Rev.*, 2012, **41**, 8099.
5 R. Ferrando, J. Jellinek and R. L. Johnston, *Chem. Rev.*, 2008, **108**, 845–910.
6 (*a*) I. N. Francesco, F. Fontaine-Vive and S. Antoniotti, *ChemCatChem*, 2014, **6**, 2784; (*b*) S. Guo, S. Zhang and S. Sun, *Angew. Chem., Int. Ed.*, 2013, **52**, 8526.
7 (*a*) V. Mazumder, Y. Lee and S. Sun, *Adv. Funct. Mater.*, 2010, **20**, 1224; (*b*) X. Liu, D. Wang and Y. Li, *Nano Today*, 2012, **7**, 448.
8 (*a*) N. Miyaura and A. Suzuki, *Chem. Rev.*, 1995, **95**, 2457; (*b*) E. Dirent and H. M. Budzelaar, *Chem. Rev.*, 1996, **96**, 663; (*c*) F. Bellina, A. Carpita and R. Rossi, *Synthesis*, 2004, **15**, 2419; (*d*) L. Yin and J. Liebscher, *Chem. Rev.*, 2007, **107**, 133.
9 S. F. Ho, A. Mendoza-Garcia, S. Guo, D. Su, S. Liu, Ö. Metin and S. Sun, *Nanoscale*, 2014, **6**, 6970.
10 H. Göksu, S. F. Ho, Ö. Metin, K. Korkmaz, A. Mendoza-Garcia, M. S. Gültekin and S. Sun, *ACS Catal.*, 2014, **4**, 1777.
11 S. Diyarbakır, H. Can and Ö. Metin, *ACS Appl. Mater. Interfaces*, 2015, **7**, 3199.

12 H. U. Blaser, A. Baiker and R. Prins, in *Heterogeneous Catalysis and Fine Chemicals*, ed. H. U. Blaser and E. Schmidt, Elsevier, Amsterdam, 1997, vol. 9, p. 17.
13 G. W. Kabalka and R. S. Varma, Reduction of Nitro and Nitroso Compounds, in *Comprehensive Organic Synthesis*, ed. B. M. Trost and I. Fleming, Pergamon, Oxford, 1991, vol. 1, p. 363.
14 (*a*) D. C. Gowda and B. Mahesh, *Synth. Commun.*, 2000, **30**, 3639; (*b*) M. C. Kimber, A. C. Try, L. Painter, M. M. Harding and P. Turner, *J. Org. Chem.*, 2000, **65**, 3042.
15 H. U. Blaser, H. Steiner and M. Studer, *ChemCatChem*, 2009, **1**, 210.
16 (*a*) S. Gladiali and G. Mestroni, in *Transition Metals for Organic Synthesis*, ed. M. Beller and C. Bolm, Wiley-VCH, Weinheim, 2004, vol. 1, p. 145; (*b*) S. Gladiali and E. Alberico, *Chem. Soc. Rev.*, 2006, **35**, 226; (*c*) J. S. M. Samec, J.-E. Backvall, P. G. Andersson and P. Brandt, *Chem. Soc. Rev.*, 2006, **35**, 237.
17 M. Kumarraja and K. Pitchumani, *Appl. Catal., A*, 2004, **265**, 135.
18 S. K. Mohapatra, S. U. Sonavane, R. V. Jayaram and P. Selvam, *Tetrahedron Lett.*, 2002, **43**, 8527.
19 (*a*) A. Wolfson, C. Dlugy, Y. Shotland and D. Tavor, *Tetrahedron Lett.*, 2009, **50**, 5951; (*b*) M. B. Gawande, A. K. Rathi, P. S. Branco, I. D. Nogueira, A. Velhinho, J. J. Shrikhande, U. U. Indulkar, R. V. Jayaram, C. A. A. Ghumman, N. Bundaleski and O. M. N. D. Teodoro, *Chem. – Eur. J.*, 2012, **18**, 12628.
20 K. Prasad, X. Jiang, J. S. Slade, J. Clemens, O. Repic and T. J. Blacklock, *Adv. Synth. Catal.*, 2005, **347**, 1769.
21 B. Peng and J. Chen, *Energy Environ. Sci.*, 2008, **1**, 479–483.
22 H. Göksu, H. Can, K. Şendil, M. S. Gültekin and Ö. Metin, *Appl. Catal., A*, 2014, **488**, 176.
23 (*a*) Y. Hou, H. Kondoh, T. Kogure and T. Ohta, *Chem. Mater.*, 2004, **16**, 5149; (*b*) I. Castellanos-Rubio, M. Insausti, I. G. Muro, D. C. Arias-Duque, J. C. Hernandez-Garrido, T. Rojo and L. Lezama, *J. Nanopart. Res.*, 2015, **17**, 229.
24 A. L. Peterson, *Phys. Rev.*, 1939, **56**, 978.
25 B. Kılıç, S. Sencanlı and Ö. Metin, *J. Mol. Catal. A: Chem.*, 2012, **361-362**, 104.
26 T. Yamashita and P. Hayes, *Appl. Surf. Sci.*, 2008, **254**, 2441–2449.
27 M. C. Biesinger, B. P. Payne, A. P. Grosvenor, L. W. M. Lau, A. R. Gerson and R. C. Smart, *Appl. Surf. Sci.*, 2011, **257**, 2717–2730.
28 Y. Zhang, X. He, J. Ouyang and H. Yang, *Sci. Rep.*, 2013, **3**, 1–5.
29 See the supporting information on the structures of by-products and the related NMR spectra.
30 (*a*) G. W. Kabalka and R. S. Varma, Reduction of Nitro and Nitroso Compounds, in *Comprehensive Organic Synthesis: selectivity, strategy and efficiency in modern organic chemistry*, ed. B. M. Trost and I. Feleming, Pergamon Press, Oxford, UK, 1991, vol. 8; (*b*) A. Tungler, T. Tarnai, L. Hegadus, K. Fodor and T. Mathe, *Platinum Met. Rev.*, 1998, **42**, 108–115.
31 A. Agrawal and P. Tratnyek, *Environ. Sci. Technol.*, 1996, **30**, 153–160.
32 N. Toshima, H. Yah and Y. Shiraishi, Recent Progress in Bimetallic Nanoparticles: Their Preparation, Structures and Functions, in *Metal Nanoclusters in Catalysis and Materials Science: The Issue of Size Control*, ed. B. Corain, G. Schmid and N. Toshima, Elsevier, Amsterdam, Netherlands, 2008.
33 K. J. Bryden and J. Y. Ying, *J. Membr. Sci.*, 2002, **203**, 29–42.
34 (*a*) W. S. Hummers and R. E. Offeman, *J. Am. Chem. Soc.*, 1958, **80**, 1339; (*b*) N. I. Kovtyukhova, P. J. Ollivier, B. R. Martin, T. E. Mallouk, S. A. Chizhik, E. V. Buzaneva and A. D. Gorchinskiy, *Chem. Mater.*, 1999, **11**, 771.
35 K. L. Ai, Y. L. Liu, L. H. Lu, X. L. Cheng and L. H. Huo, *J. Mater. Chem.*, 2011, **21**, 3365.
36 (*a*) Ö. Metin, E. Kayhan, S. Özkar and J. J. Schenieder, *Int. J. Hydrogen Energy*, 2012, **37**, 8161; (*b*) Ö. Metin, Ş. Aydoğan and K. Meral, *J. Alloys Compd.*, 2014, **585**, 681.